

# Performance Evaluation of Ising and QUBO Variable Encodings in Boltzmann Machine Learning

Yasushi Hasegawa<sup>1,2\*</sup>, and Masayuki Ohzeki<sup>1,3,4,5</sup>

<sup>1</sup>*Graduate School of Information Sciences, Tohoku University, Sendai 980-8579, Japan*

<sup>2</sup>*Technology Strategy Division, SCSK Corporation, Koto, Tokyo 135-8110, Japan*

<sup>3</sup>*Department of Physics, Institute of Science Tokyo, Meguro, Tokyo 152-8551, Japan*

<sup>4</sup>*Research and Education Institute for Semiconductors and Informatics, Kumamoto University, Chuo, Kumamoto 860-0862, Japan,*

<sup>5</sup>*Sigma-i Co., Ltd., Minato, Tokyo 108-0075, Japan*

We compare Ising ( $\{-1, +1\}$ ) and QUBO ( $\{0, 1\}$ ) encodings for Boltzmann machine learning under a controlled protocol that fixes the model, sampler, and step size. Exploiting the identity that the Fisher information matrix (FIM) equals the covariance of sufficient statistics, we visualize empirical moments from model samples and reveal systematic, representation-dependent differences. QUBO induces larger cross terms between first- and second-order statistics, creating more small-eigenvalue directions in the FIM and lowering spectral entropy. This ill-conditioning explains slower convergence under stochastic gradient descent (SGD). In contrast, natural gradient descent (NGD)—which rescales updates by the FIM metric—achieves similar convergence across encodings due to reparameterization invariance. Practically, for SGD-based training, the Ising encoding provides more isotropic curvature and faster convergence; for QUBO, centering/scaling or NGD-style preconditioning mitigates curvature pathologies. These results clarify how representation shapes information geometry and finite-time learning dynamics in Boltzmann machines and yield actionable guidelines for variable encoding and preprocessing.

## 1. Introduction

Binary systems in combinatorial optimization and energy-based learning are commonly formulated as the Ising model ( $s \in \{-1, +1\}$ ) or the Quadratic Unconstrained Binary Optimization (QUBO) model ( $x \in \{0, 1\}$ ). The two encodings are related by the affine transforma-

---

\*hasegawa.yasushi.s6@dc.tohoku.ac.jp

tion  $s = 2x - 1$  and are theoretically equivalent to their optimal solutions.<sup>1,2)</sup> With appropriate parameter mapping, either representation can reach the same ground state of a given problem.

However, in practical optimization and learning dynamics, this equivalence breaks down. Variable encoding, scaling, and penalty design differences can lead to markedly distinct convergence behaviors and robustness. For example, studies on the Fujitsu Digital Annealer have shown that solving the same problem using Ising and QUBO formulations can yield smoother and more stable trajectories under the Ising representation.<sup>3)</sup> Similarly, comparing QUBO transformation schemes for 3-SAT demonstrates that the transformation significantly affects solution quality on identical hardware.<sup>4)</sup> In Ising-machine-based solvers for linear systems, the choice of real-number encoding also influences accuracy and error characteristics, reflecting differences in search geometry and the ease of crossing energy barriers.<sup>5)</sup> These observations collectively indicate that even for the same logical problem, the coordinate system—i.e., the representation—can strongly affect finite-time optimization behavior.

This issue naturally extends to Boltzmann Machine (BM) learning,<sup>6)</sup> where iterative, sampling-based training methods such as Contrastive Divergence rely on accurate gradient estimates. The distribution output by a quantum annealer, due to freeze-out effects, can often be modeled as a Gibbs–Boltzmann form; hence, annealers have been used as physical samplers for BM and Restricted Boltzmann Machine (RBM) learning.<sup>7–9)</sup> In classical and quantum settings, gradient scale and data centering influence convergence through conditioning and gradient variance.<sup>10–12)</sup> The Ising encoding naturally offers zero-mean centering and symmetric scaling of interaction terms, which can reduce bias and variance in gradient estimates and facilitate step-size tuning. In contrast, the QUBO encoding lacks this centering property. From an information-geometric perspective, switching from QUBO to Ising effectively performs centering and rescaling equivalent to preconditioning by the Fisher information matrix (FIM).<sup>13,14)</sup>

Natural Gradient Descent (NGD) addresses curvature anisotropy by rescaling updates using the FIM metric. Both theoretical and empirical studies show that NGD accelerates and stabilizes learning compared with first-order methods.<sup>12,13,15)</sup> Investigating how encoding-dependent changes in the FIM spectrum affect convergence thus provides a principled way to understand the influence of variable representation on learning dynamics.

This study systematically examines how variable encoding—Ising versus QUBO—affects convergence and conditioning in Boltzmann Machine learning under strictly controlled conditions, fixing the model, sampler, and learning rate design. We analyze the relationship between encoding and the information-geometric curvature characterized by FIM spectra and

spectral entropy. By comparing Stochastic Gradient Descent (SGD) and Natural Gradient Descent (NGD), we clarify how encoding and learning rules interact to determine convergence speed and stability. Our findings yield practical insights into preprocessing strategies (centering and scaling) and representation choice for efficient Boltzmann Machine learning.

The following section introduces the Ising and QUBO formulations, the Boltzmann Machine model, and the SGD and NGD update rules. The Results section presents learning trajectories and FIM spectral analyses for both encodings. Finally, the Conclusion summarizes the key findings and outlines future research directions.

## 2. Methods

### 2.1 Model and Representations

We consider the same learner (fully connected Boltzmann Machine), the same sampler (Simulated Annealing (SA)), and the same update rules (SGD/NGD), and vary only the variable representation: Ising  $\{-1, +1\}$  versus QUBO  $\{0, 1\}$ . The Ising energy is

$$E_{\text{Ising}}(\mathbf{s}; \mathbf{h}, \mathbf{J}) = \sum_i h_i s_i + \sum_{i < j} J_{ij} s_i s_j. \quad (1)$$

The QUBO energy is

$$E_{\text{QUBO}}(\mathbf{x}; \mathbf{Q}) = \sum_{i \leq j} Q_{ij} x_i x_j. \quad (2)$$

The two representations are related by  $s = 2x - 1$ , which gives the following parameter correspondence (constant terms omitted):

$$h_i = \frac{1}{4} \sum_j (Q_{ij} + Q_{ji}), \quad J_{ij} = \frac{1}{4} Q_{ij}. \quad (3)$$

### 2.2 Boltzmann Machine

At temperature  $T$  (inverse temperature  $\beta = 1/T$ ), the Gibbs–Boltzmann distribution is

$$P_\theta(\mathbf{s}) = \frac{1}{Z(\theta)} \exp\{-\beta E_{\text{Ising}}(\mathbf{s}; \theta)\}, \quad (4)$$

$$Z(\theta) = \sum_{\mathbf{s}} \exp\{-\beta E_{\text{Ising}}(\mathbf{s}; \theta)\}, \quad (5)$$

and analogously for QUBO. The average log-likelihood  $L(\theta) = \frac{1}{N} \sum_{n=1}^N \log P_\theta(\mathbf{s}^n)$  has gradient

$$\nabla L(\theta) = \beta (\mathbb{E}_{\text{data}}[\nabla_\theta E] - \mathbb{E}_{P_\theta}[\nabla_\theta E]). \quad (6)$$

Componentwise,  $\nabla_{h_i} E = s_i$ ,  $\nabla_{J_{ij}} E = s_i s_j$ , and  $\nabla_{Q_{ij}} E = x_i x_j$ . The model expectation  $\mathbb{E}_{P_\theta}[\cdot]$  is approximated by SA with single spin flips and Metropolis acceptance  $\alpha = \min\{1, \exp(-\beta \Delta E)\}$ .

### 2.3 Stochastic Gradient Descent (SGD) and Natural Gradient Descent (NGD)

A second-order Taylor approximation near  $\theta_t$  gives

$$L(\theta_t + \delta) \approx L(\theta_t) + \nabla L(\theta_t)^\top \delta + \frac{1}{2} \delta^\top \nabla^2 L(\theta_t) \delta. \quad (7)$$

At a local minimizer,  $\nabla L(\theta_t) + \nabla^2 L(\theta_t) \delta = 0$ , hence  $\delta = -(\nabla^2 L)^{-1} \nabla L$ . SGD updates

$$\theta_{t+1} = \theta_t - \eta_{\text{SGD}} \nabla L(\theta_t), \quad (8)$$

with a stability condition<sup>16)</sup>  $\rho(I - \eta \nabla^2 L) < 1$ , namely  $0 < \eta < 2/\lambda_{\max}(\nabla^2 L)$ . NGD updates

$$\theta_{t+1} = \theta_t - \eta_{\text{NGD}} (\nabla^2 L(\theta_t))^{-1} \nabla L(\theta_t). \quad (9)$$

The Hessian equals the FIM for Boltzmann distributions. In fact

$$\mathbb{E} \left[ \frac{\partial^2 \log P}{\partial \theta_i \partial \theta_j} \right] = -\mathbb{E} \left[ \frac{\partial \log P}{\partial \theta_i} \frac{\partial \log P}{\partial \theta_j} \right] = -F_{\theta}. \quad (10)$$

We thus employ a damped NGD step

$$\theta_{t+1} = \theta_t + \eta_{\text{NGD}} (F_{\theta} + \lambda I)^{-1} \nabla L(\theta_t). \quad (11)$$

Moreover, for Boltzmann distributions, the FIM equals the covariance matrix of sufficient statistics. For QUBO parameters  $Q_{ij}$ :

$$\mathbb{E} \left[ \frac{\partial \log P}{\partial Q_{ij}} \frac{\partial \log P}{\partial Q_{kl}} \right] = \mathbb{E}[(x_i x_j - \mathbb{E}[x_i x_j])(x_k x_l - \mathbb{E}[x_k x_l])] = \mathbb{E}[x_i x_j x_k x_l] - \mathbb{E}[x_i x_j] \mathbb{E}[x_k x_l]. \quad (12)$$

For Ising parameters  $h_i, J_{ij}$ :

$$\mathbb{E} \left[ \frac{\partial \log P}{\partial h_i} \frac{\partial \log P}{\partial h_j} \right] = \mathbb{E}[s_i s_j] - \mathbb{E}[s_i] \mathbb{E}[s_j], \quad (13)$$

$$\mathbb{E} \left[ \frac{\partial \log P}{\partial h_i} \frac{\partial \log P}{\partial J_{kl}} \right] = \mathbb{E}[s_i s_k s_l] - \mathbb{E}[s_i] \mathbb{E}[s_k s_l], \quad (14)$$

$$\mathbb{E} \left[ \frac{\partial \log P}{\partial J_{ij}} \frac{\partial \log P}{\partial J_{kl}} \right] = \mathbb{E}[s_i s_j s_k s_l] - \mathbb{E}[s_i s_j] \mathbb{E}[s_k s_l]. \quad (15)$$

### 2.4 Spectral Entropy

Let  $\{\lambda_i\}$  be the FIM eigenvalues. The spectral entropy is

$$S = - \sum_i \frac{\lambda_i}{\sum_j \lambda_j} \log \left( \frac{\lambda_i}{\sum_j \lambda_j} \right), \quad (16)$$

which measures the evenness of curvature allocation, attaining its maximum when all eigenvalues are equal.

## 3. Results

We compare Ising and QUBO encodings while fixing the BM (fully connected), sampler (SA with  $\beta = 1$ , 10,000 samples), and learning rate design. Datasets are: (i) Bar-and-Stripe

(BAS)  $2 \times 2$  (each pattern randomly replicated to total 450 samples); (ii) BAS  $3 \times 3$  (randomly replicated to 1,120 samples); (iii) Ising-sampled synthetic data with dimension  $d = 10$  and couplings  $J_{i>j} \sim \mathcal{N}(0, J_c^2/d)$  with  $J_c \in \{0.5, 1.0, 1.5\}$ , 2,000 samples for each. Learning rates are  $\eta_{\text{SGD}} = \frac{0.01}{\lambda_{\max}(F_\theta)}$ ,  $\eta_{\text{NGD}} = 0.01$ , with damping  $\lambda = 0.001$ , equalizing curvature scales across encodings.

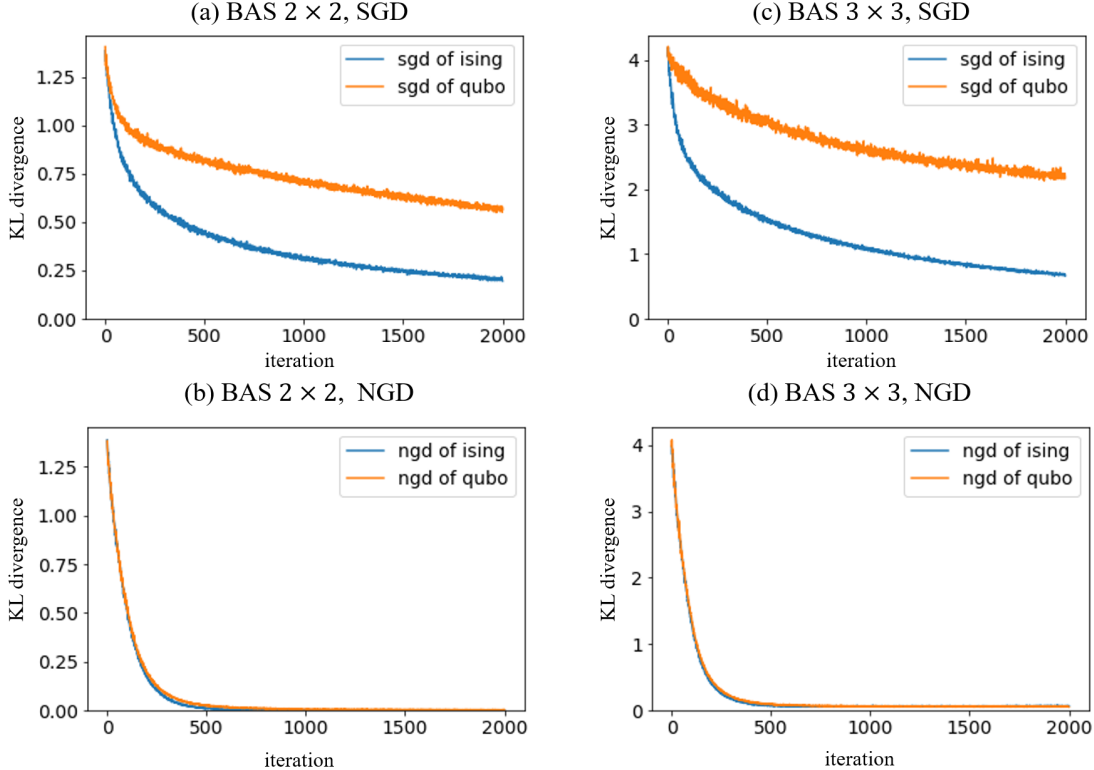


**Fig. 1.** Comparison on BAS data. Under NGD, convergence matches across encodings; under SGD, Ising reduces KL divergence faster than QUBO.

From Figures 1-6, we did not observe QUBO converging faster than Ising on any dataset. Under NGD, KL-divergence trajectories are similar across encodings. These trajectory and spectrum analyses and the spectral entropy and FIM eigenvalues indicate that the Ising encoding has larger spectral entropy and more isotropic curvature, yielding faster convergence under SGD. Proper curvature scaling (NGD) allows QUBO to achieve convergence comparable to Ising.

In QUBO, the FIM eigenvalues fall off sharply after the 11th component, and a smaller  $J_c$  extends the period during which very small eigenvalues persist. For Ising, the first-order moments  $\mathbb{E}[s_i]$  and third-order moments  $\mathbb{E}[s_i s_k s_l]$  are distributed around zero, while second- and

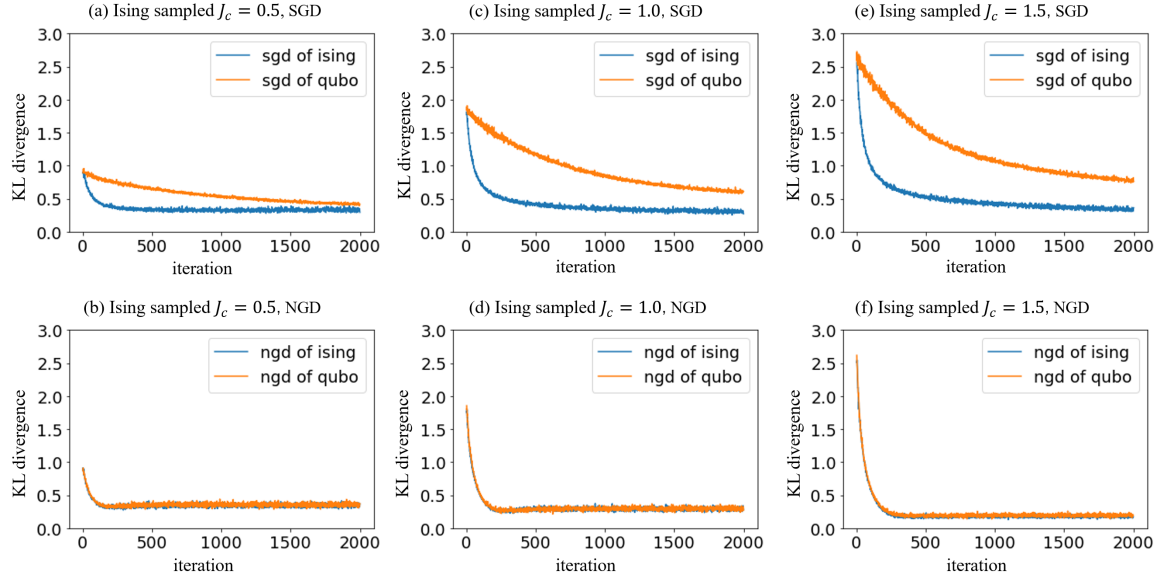


**Fig. 2.** Comparison on Ising-sampled data. NGD yields matching KL convergence; under SGD, Ising converges faster.

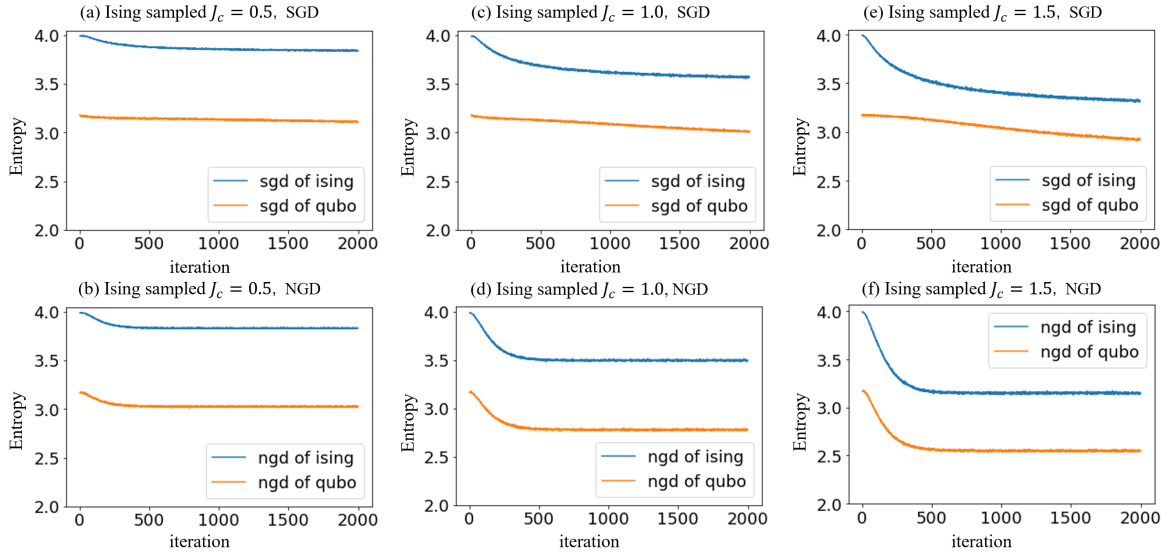


**Fig. 3.** Spectral entropy of the FIM on Ising-sampled data. Entropy is consistently larger for Ising, indicating a more even curvature allocation.

fourth-order moments  $\mathbb{E}[s_i s_j]$ ,  $\mathbb{E}[s_i s_j s_k s_l]$  are symmetric around zero. In contrast, QUBO's  $x \in \{0, 1\}$  asymmetry yields non-negative moment distributions; in particular  $\mathbb{E}[x_i] \approx 0.5$  and  $\mathbb{E}[x_i x_j] \approx 0.25$ . Consequently, in Ising the off-diagonal FIM block  $F_{h,J} = \mathbb{E}[s_i s_k s_l] - \mathbb{E}[s_i] \mathbb{E}[s_k s_l]$  is very small and the FIM is approximately block-diagonal, whereas in QUBO the off-diagonal block is non-zero.

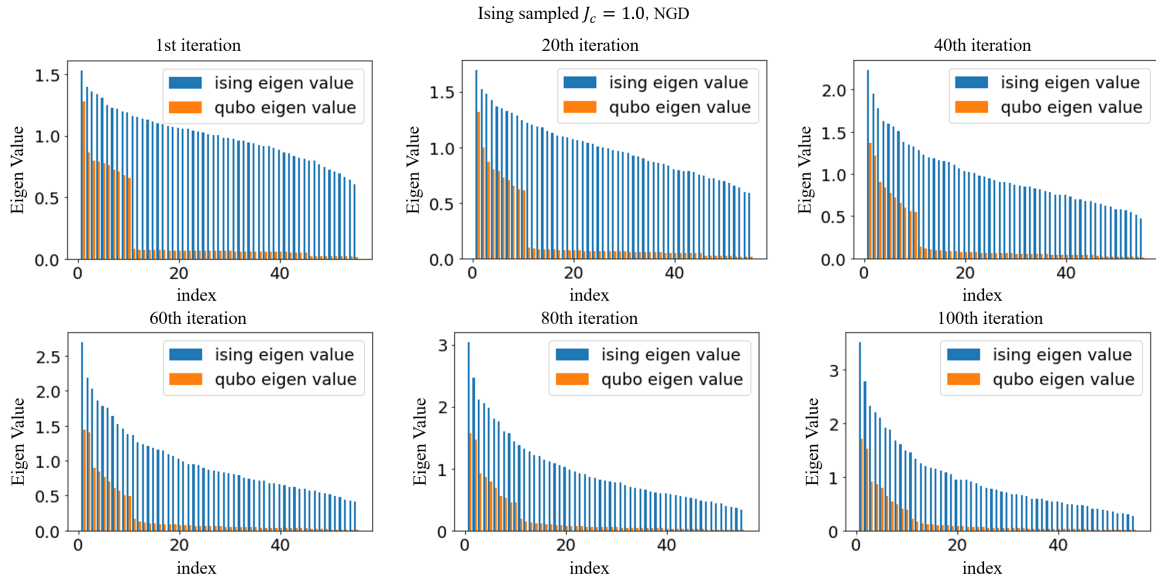


**Fig. 4.** Evolution of FIM eigenvalues on Ising-sampled data ( $J_c = 1.0$ ). Ising exhibits larger and more dispersed eigenvalues; QUBO shows a split between large and very small eigenvalues early in training.

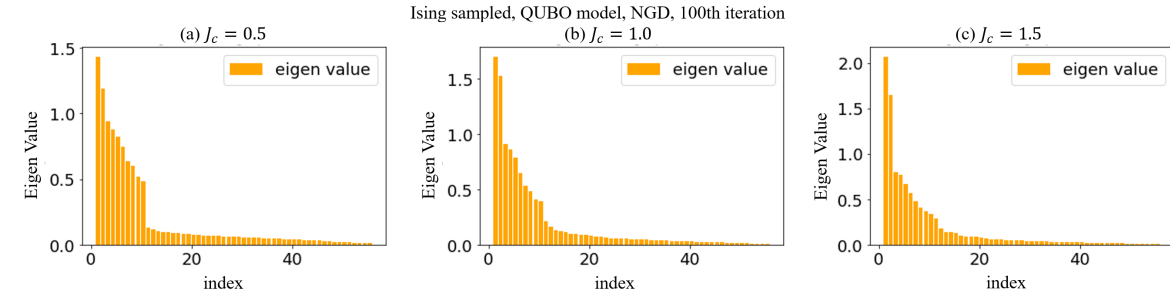


**Fig. 5.** FIM eigenvalues for QUBO (NGD, the 100th iteration). A smaller  $J_c$  prolongs the period with extremely small eigenvalues.

Writing the FIM in block form for first- and second-order parameters,

$$F_\theta = \begin{pmatrix} F_{11} & F_{12} \\ F_{21} & F_{22} \end{pmatrix}, \quad (17)$$

the Schur bounds its minimum eigenvalue complement inequality<sup>16,17)</sup>

$$\lambda_{\min}(F_\theta) \leq \lambda_{\min}(F_{22} - F_{21}F_{11}^{-1}F_{12}). \quad (18)$$

Since  $F_{12} = F_{21} \approx 0$  for Ising while it is non-zero for QUBO, the latter tends to produce smaller eigenvalues.

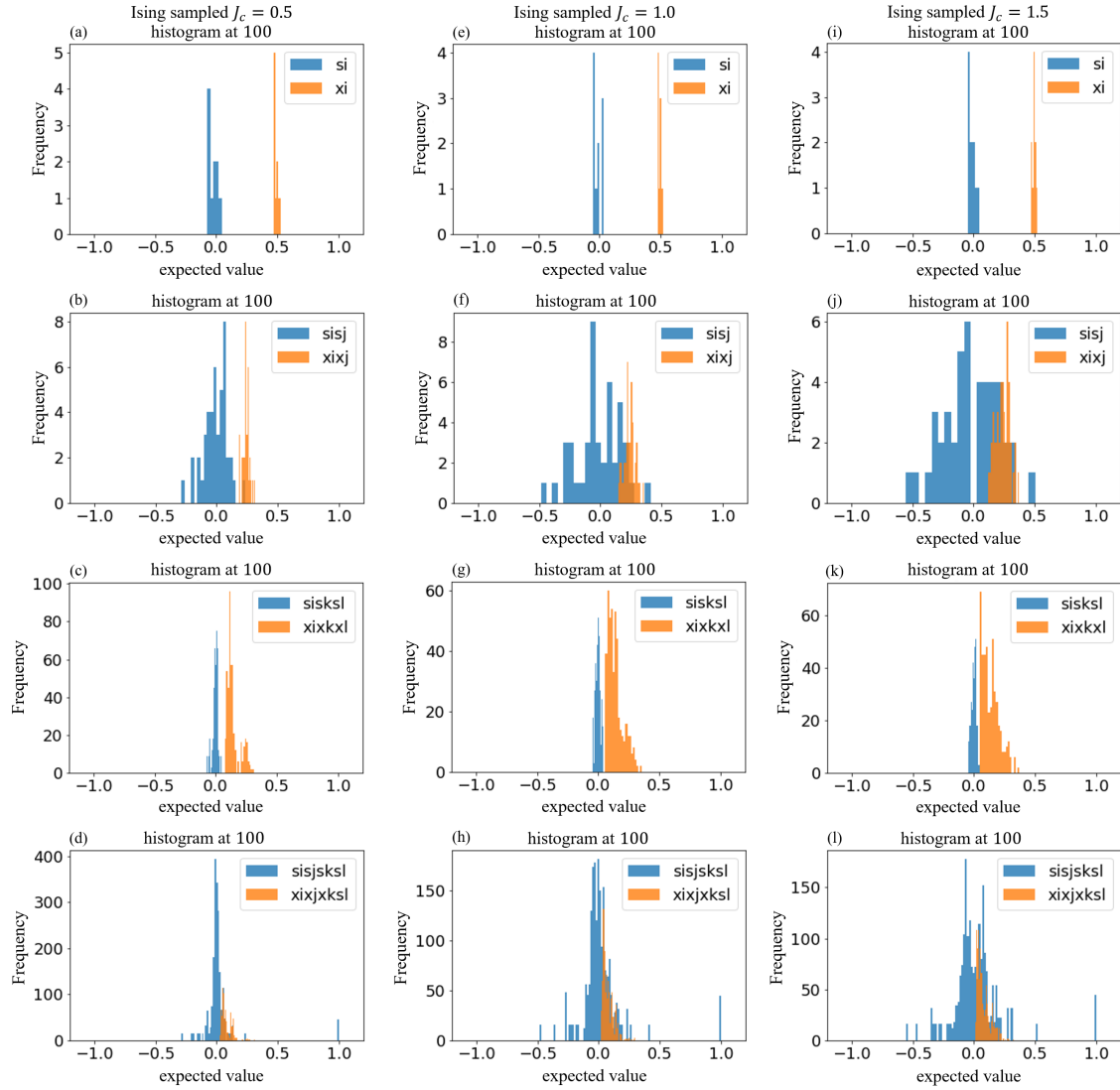


**Fig. 6.** Histograms of expectations for Ising ( $\mathbb{E}[s_i]$ ,  $\mathbb{E}[s_i s_j]$ ,  $\mathbb{E}[s_i s_k s_l]$ ,  $\mathbb{E}[s_i s_j s_k s_l]$ ) and QUBO ( $\mathbb{E}[x_i]$ ,  $\mathbb{E}[x_i x_j]$ ,  $\mathbb{E}[x_i x_k x_l]$ ,  $\mathbb{E}[x_i x_j x_k x_l]$ ) at iteration 100 under NGD. Ising distributions are centered around zero; QUBO’s  $\mathbb{E}_{p_\theta}[x_j]$  concentrates near 0.5 and  $\mathbb{E}_{p_\theta}[x_i x_j]$  near 0.25. While  $\mathbb{E}[s_i]$ ,  $\mathbb{E}[x_j]$ , and  $\mathbb{E}[s_i s_k s_l]$  remain stable as  $J_c$  varies, the variance of  $\mathbb{E}_{p_\theta}[s_i s_j]$ ,  $\mathbb{E}_{p_\theta}[s_i s_k s_l]$ ,  $\mathbb{E}_{p_\theta}[x_i x_j]$ ,  $\mathbb{E}_{p_\theta}[x_i x_k x_l]$ , and  $\mathbb{E}_{p_\theta}[x_i x_j x_k x_l]$  increases with  $J_c$ .

#### 4. Conclusion

We presented a unified analysis of Boltzmann Machine learning dynamics from an information-geometric perspective, comparing the Ising ( $\{-1, +1\}$ ) and QUBO ( $\{0, 1\}$ ) representations while fixing the model, sampler, and learning rate design. This setup isolates the effect of variable encoding on convergence behavior and the Fisher information spectrum.

The main findings are summarized as follows:

- **Stochastic Gradient Descent (SGD):** The Ising encoding consistently achieves faster

Kullback–Leibler (KL) divergence reduction and requires fewer iterations to converge than QUBO. This advantage arises from better numerical conditioning, as QUBO introduces parameterization-dependent gradient scales and cross-correlations that increase curvature anisotropy.

- **Natural Gradient Descent (NGD):** When curvature is properly accounted for via the Fisher information matrix (FIM) metric, convergence behavior becomes nearly identical across encodings. This demonstrates that NGD effectively restores representation invariance by rescaling updates according to local geometry.
- **Fisher Information Spectra:** During training, the FIM exhibits (a) strong anisotropy in early iterations, (b) progressive redistribution of spectral mass, and (c) systematically smaller eigenvalues and lower spectral entropy for QUBO. These characteristics originate from persistent cross-block correlations between first- and second-order sufficient statistics.

The Ising encoding provides more isotropic curvature and better-conditioned learning under SGD, leading to faster convergence. NGD further enhances both stability and speed for either encoding, though it requires computing or approximating  $F^{-1}$ , whose cost scales with parameter dimensionality. Efficient second-order approximations—such as block-diagonal or low-rank FIMs, Kronecker-factored curvature (K-FAC), or stochastic inverse estimators like Hutchinson, Lanczos, Shampoo, and AdaHessian methods<sup>14, 18–21)</sup>—offer promising routes to scalable NGD implementations.

Because the FIM of a Boltzmann Machine equals the covariance of sufficient statistics, initialization and preprocessing that align first- and second-order moments (centering and scaling) can substantially reduce training iterations, especially for QUBO variables. Future research directions include: (i) principled moment-matching initialization schemes, (ii) adaptive damping policies informed by spectral monitoring, (iii) hardware-aware studies using quantum and digital annealers—including online calibration of the effective inverse temperature for quantum annealing–based RBM training,<sup>22)</sup> and (iv) extensions to deep energy-based models where variable representation interacts with hierarchical structure, as suggested by three-layer RBM kernel learning and the three-layer QDRBM.<sup>8, 23)</sup>

## Acknowledgment

We received financial support from the Cabinet Office programs for bridging the gap between R&D and IDEal society (Society 5.0), Generating Economic and Social Value (BRIDGE), and the Cross-ministerial Strategic Innovation Promotion Program (SIP)

(No. 23836436).

## References

- 1) A. Lucas: *Frontiers in physics* **2** (2014) 5.
- 2) F. Glover, G. Kochenberger, R. Hennig, and Y. Du: *Annals of Operations Research* **314** (2022) 141.
- 3) Z. Kaseb, M. Möller, P. P. Vergara, and P. Palensky: *Scientific Reports* **14** (2024) 23216.
- 4) C. Münch, F. Schinkel, S. Zielinski, and S. Walter: arXiv preprint arXiv:2312.11645 (2023).
- 5) K. Endo, Y. Matsuda, S. Tanaka, and M. Muramatsu: *PloS one* **19** (2024) e0304594.
- 6) D. H. Ackley, G. E. Hinton, and T. J. Sejnowski: *Cognitive science* **9** (1985) 147.
- 7) T. Sato, M. Ohzeki, and K. Tanaka: *Scientific reports* **11** (2021) 13523.
- 8) Y. Hasegawa, H. Oshiyama, and M. Ohzeki: arXiv preprint arXiv:2304.10144 (2023).
- 9) M. Urushibata, M. Ohzeki, and K. Tanaka: *Journal of the Physical Society of Japan* **91** (2022) 074008.
- 10) G. Montavon and K.-R. Müller, Deep Boltzmann machines and the centering trick, *Neural Networks: Tricks of the Trade*: Second Edition, pp. 621–637. Springer, 2012.
- 11) G. E. Hinton, A practical guide to training restricted Boltzmann machines, *Neural Networks: Tricks of the Trade*: Second Edition, pp. 599–619. Springer, 2012.
- 12) J. Melchior, A. Fischer, and L. Wiskott: *Journal of Machine Learning Research* **17** (2016) 1.
- 13) S.-I. Amari: *Neural computation* **10** (1998) 251.
- 14) J. Martens and R. Grosse: *International conference on machine learning*, 2015, pp. 2408–2417.
- 15) G. Desjardins, R. Pascanu, A. Courville, and Y. Bengio: arXiv preprint arXiv:1301.3545 (2013).
- 16) R. A. Horn and C. R. Johnson: *Matrix analysis* (Cambridge university press, 2012).
- 17) R. L. Smith: *Linear algebra and its applications* **177** (1992) 137.
- 18) M. F. Hutchinson: *Communications in Statistics-Simulation and Computation* **18** (1989) 1059.
- 19) V. Gupta, T. Koren, and Y. Singer: *International Conference on Machine Learning*, 2018, pp. 1842–1850.

- 20) Z. Yao, A. Gholami, S. Shen, M. Mustafa, K. Keutzer, and M. Mahoney: proceedings of the AAAI conference on artificial intelligence, Vol. 35, 2021, pp. 10665–10673.
- 21) S. Ubaru, J. Chen, and Y. Saad: SIAM Journal on Matrix Analysis and Applications **38** (2017) 1075.
- 22) T. Goto and M. Ohzeki: Journal of the Physical Society of Japan **94** (2025) 034002.
- 23) K. Yonaga and M. Ohzeki: Journal of the Physical Society of Japan **94** (2025) 053002.